

# Comparison of Image Reconstruction Algorithms for the Depiction of Vessel Anatomy in PC VIPR Datasets

A. G. Anderson<sup>1</sup>, K. M. Johnson<sup>2</sup>, J. Bock<sup>3</sup>, M. Markl<sup>3</sup>, and O. Wieben<sup>2,4</sup>

<sup>1</sup>Biomedical Engineering, University of Wisconsin, Madison, WI, United States, <sup>2</sup>Medical Physics, University of Wisconsin, Madison, WI, United States, <sup>3</sup>Diagnostic Radiology, Medical Physics, University Hospital Freiburg, Freiburg, Germany, <sup>4</sup>Radiology, University of Wisconsin, Madison, WI, United States

**Introduction:** Recently, volumetric cine phase contrast MR Angiography (PC MRA) acquisitions with 3D flow encoding have become feasible by reducing the required acquisition times with the introduction of advanced imaging technologies such as faster gradients, parallel imaging, respiratory motion compensation [4], radially undersampled trajectories [2], exploration of redundancies in dynamic k-space [1] and others. Due to the possible linking of nephrogenic systemic fibrosis (NFS) and gadolinium-based MR contrast agents, there is renewed interest in such non-contrast enhanced MRA approaches. While these data provide detailed anatomical and functional information, the corresponding image amount of hundreds or thousands of images poses challenges for data management. It is often desirable to represent these data in a comprehensive fashion for the visualization of the vasculature. In addition, knowledge of the exact vessel boundaries is essential for the derivation of additional hemodynamic parameters such as wall shear stress or pressure gradients from the velocity fields. Here we compare several approaches for the generation of such PC angiography datasets from high resolution PC VIPR acquisitions [2].

**Methods:** Four renal PC VIPR data sets (two patients, two healthy volunteers) were acquired on a clinical 3T system (GE Healthcare) with a radially undersampled, dual echo sequence with balanced bipolar gradients and adaptive respiratory gating [3]. Common imaging parameters include: receiver bandwidth = 62.5 kHz, subject adapted VENC of 40-60 cm/s, imaging volume = 320 x 320 x 320 mm<sup>3</sup>, readout = 256-320, TR/TE = 9.6ms/3.4ms, isotropic spatial resolution = (1-1.25 mm)<sup>3</sup>, scan time: approximately 10 min scan time with 50% respiratory gating efficiency. Retrospective ECG gating was used with a view sharing like approach for 3D radial imaging to reconstruct magnitude and 3 velocity datasets for 17 cardiac phases for each subject (see Fig. 1). Several algorithms were implemented in C++ to generate a single angiogram from these datasets in form of a DICOM series: (I) A piecewise pseudo complex difference reconstruction technique that allows for velocity threshold adjustment  $M \sin[\pi|v|/(2venc)]$ ,  $|v| < v_{enc}$ . For this comparison the velocity threshold was set high enough that the function represented a one-to-one map of absolute velocity average. (II) Absolute velocity was weighted with the magnitude for each time frame, and combined over all cardiac phases as a sum of squares  $\sqrt{\sum (V_i * M_i)^2}$ . (III) Another sum of squares method where the velocity is squared before weighting  $\sqrt{\sum (V_i^2 * M_i)^2}$ . (IV) Classical magnitude weighting (also

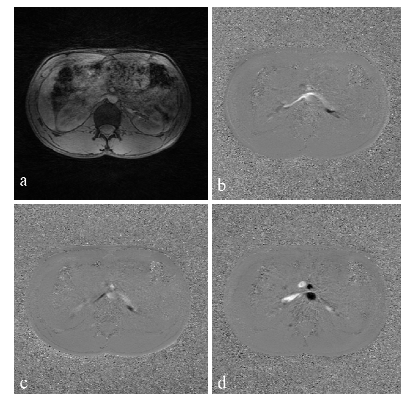


**Fig. 1:** Axial slice from a renal PC VIPR exam showing the corresponding magnitude (a) and the three velocity components vx (b), vy (c), and vz (d).

called masking) accomplished by multiplication of the average absolute velocity with the average magnitude  $(\bar{V}) * (\bar{M})$ . (V) A similar masking method, this time with absolute velocity average weighted with the average of the magnitude squared  $(\bar{V}) * (\bar{M}^2)$ . (VI) Another masking approach with both the velocity and the magnitude squared  $(\bar{V}^2) * (\bar{M}^2)$ . (VII) A basic average of absolute velocity weighted with average magnitude  $(\bar{V} * \bar{M})$ . (VIII) A similar basic approach with the magnitude squared  $(\bar{V} * \bar{M}^2)$ . For quantitative image comparison, a circular ROI was selected within the abdominal aorta approximately 1 cm proximal to the renal arteries. Mean and standard deviation of the ROI were used to establish relative SNR values for the algorithms. Each method was also given a subjective image quality grade (1-15) based on 1-5 points for each of the following categories: background tissue levels, ability to distinguish distal vessels, and sharpness of vessels.

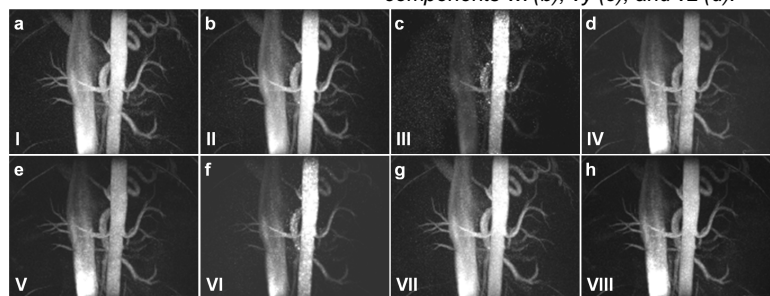


**Fig. 2:** Representative results of the eight algorithms for a healthy volunteer displayed as coronal MIP images.

**Table 1:** Relative SNR values and quality grades for the eight algorithms.

|              | I   | II    | III  | IV  | V     | VI   | VII  | VIII |
|--------------|-----|-------|------|-----|-------|------|------|------|
| Relative SNR | 7.1 | 10.8  | 5.8  | 8.1 | 8.1   | 5.4  | 11.2 | 8.5  |
| Grade        | 13  | 12.75 | 9.25 | 12  | 10.75 | 8.75 | 13   | 11.5 |

**Results:** Results from a representative study are shown in Fig. 2 for all eight algorithms. Noise amplifications and the absence of smaller vessels are apparent in methods III and VI, while methods I and VII performed best in this case. Table 1 contains average relative SNR values and subjective image quality grades for the eight calculation methods from all four subjects.

**Discussion:** Our preliminary results demonstrate significant differences in the angiograms generated by the various algorithms. We conclude that the algorithm I is best suited for the calculation of renal angiograms obtained with PC VIPR, which has unique SNR and artifact properties from the severe radial undersampling. Further studies are warranted to compare the accuracy of the geometrical representation with CE-MRA examinations and to evaluate the algorithms in other vascular territories.

**Acknowledgements:** We gratefully acknowledge GE Healthcare for their assistance and support.

**References:** [1] C Baltes et al, MRM 54:1430-8, 2005 [2] T. Gu et al., ASNR 26:743-9, 2005 [3] KM Johnson et al, ISMRM 2007, 3116. [4] M Markl et al., JCAT 28(4): 459-68, 2004